Preparation, Crystallization Behavior, and Dynamic Mechanical Property of Nanocomposites Based on Poly(vinylidene fluoride) and Exfoliated Graphite Nanoplate

Fuan He,[1] Jintu Fan,[1] Sienting Lau,[2] Laiwa Helen Chan[2]

[1]*Institute of Textiles and Clothing, The Hong Kong Polytechnic University, Hung Hom, Kowloon, Hong Kong, China*
[2]*Department of Applied Physics and Materials Research Centre, The Hong Kong Polytechnic University, Hung Hom, Kowloon, Hong Kong, China*

Received 13 March 2010; accepted 9 May 2010
DOI 10.1002/app.32801
Published online 30 July 2010 in Wiley Online Library (wileyonlinelibrary.com).

ABSTRACT: Nanocomposites based on poly(vinylidene fluoride) (PVDF) and exfoliated graphite nanoplate (xGnP) were prepared by solution precipitation method. The resulting nanocomposites were investigated with respect to their structure and properties by scanning electron microscopy (SEM), transmission electron microscopy (TEM), differential scanning calorimetry (DSC), wide-angle X-ray diffraction, and dynamic mechanical analysis. Both SEM and TEM examinations confirmed the good dispersion of xGnP in the PVDF matrix. The nonisothermal crystallization behavior of the PVDF/xGnP nanocomposites was studied using DSC technique at various cooling rates. The results indicated that the xGnPs in nanometer size might act as nucleating agents and accelerated the overall nonisothermal crystallization process. Meanwhile, the incorporation of xGnP significantly improved the storage modulus of the PVDF/xGnP nanocomposites. © 2010 Wiley Periodicals, Inc. J Appl Polym Sci 119: 1166–1175, 2011

Key words: poly(vinylidene fluoride); exfoliated graphite nanoplate; nanocomposites; crystallization behavior; dynamic mechanical property

INTRODUTION

In recent years, polymer/silicate nanocomposites have attracted a lot of interest because they exhibit improved properties in comparison with pristine polymers and conventional composites.[1–6] Nevertheless, silicate-reinforced polymers do not show significant electrical conductivity relative to other functional polymer composites containing conductive fillers, which greatly limits their application range. Exfoliated graphite nanoplate (xGnP),[7] namely, layered graphite in its exfoliated state, has good electrical and thermal conductivity, high mechanical strength, large aspect ratio, and layered structure with nanoscale thickness just like silicates. Because of these outstanding features, xGnP has been considered as a promising alternative to the commonly used silicate for the preparation of polymeric nanocomposites. Recently, the nanoscale dispersions of graphite nanoplate into various polymer matrices such as poly(methyl methacrylate) (PMMA),[8] poly (3-hydroxybutyrate) (PHB),[9] poly(styrene-*co*-acrylonitrile),[10] nylon 6,[11] polypropylene,[12] nitrile-butadiene rubber (NBR),[13] and poly(methyl acrylic acid)[14] have been reported.

Poly(vinylidene fluoride) (PVDF) has received considerable attention because of its good mechanical properties, resistance to chemicals, high dielectric permittivity, and unique pyroelectric and piezoelectric properties.[15,16] We believed that the homogeneous incorporation of graphite nanoplate into PVDF matrix can not only obtain the similar reinforcing effect of layered silicate but also impart some functional properties to the resulting nanocomposites, such as high dielectric permittivity and good electrical and thermal conductivities, which may have better potential for many applications. In our previous study, novel PVDF/xGnP nanocomposites were prepared by a solution-cast and hot-press method.[17] It was found that the incorporation of xGnP in the PVDF matrix could effectively enhance the dielectric constant of PVDF/xGnP nanocomposite with very low percolation threshold.

Correspondence to: J. Fan (tcfanjt@inet.polyu.edu.hk).
Contract grant sponsor: Research Grant Council of HKSAR (CERG Project); contract grant number: PolyU 5164/06E.
Contract grant sponsor: Hong Kong Polytechnic University (Niche Area Project); contract grant number: 1-BB82.
Contract grant sponsor: Postdoctoral Fellowship of Hong Kong Polytechnic University; contract grant number: G-YX1K.

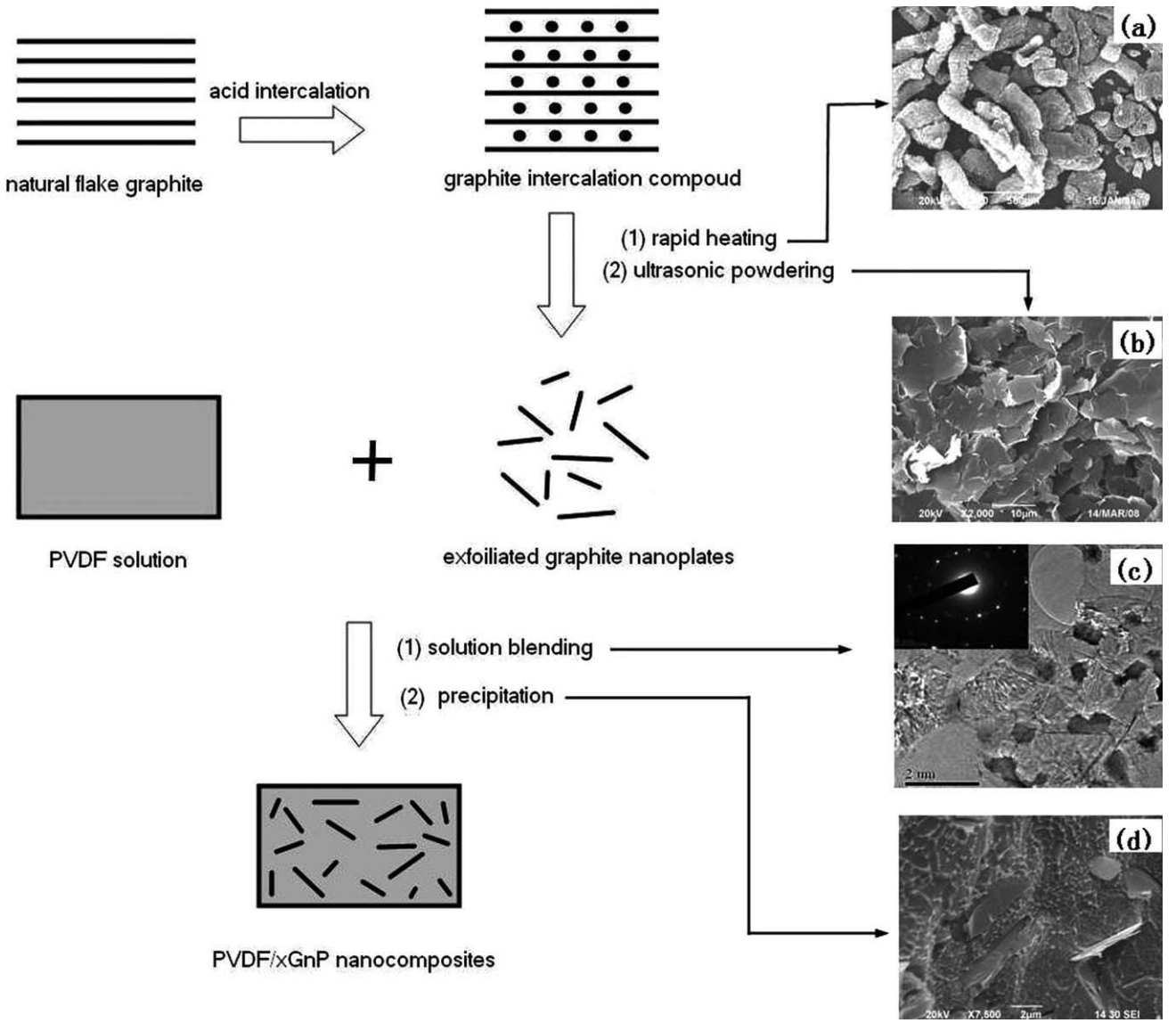

Figure 1 Schematic illustration of mechanism for formation of PVDF/xGnP nanocomposites. SEM images of (a) expandable graphite and (b) exfoliated graphite nanosheet, (c) TEM image of PVDF/xGnP nanocomposites, and (d) SEM image of PVDF/xGnP nanocomposites.

In this work, we attempt to fabricate nanocomposites consisting of PVDF and xGnPs by a solution precipitation method. The effect of different concentrations of graphite nanoplates on the morphology, nonisothermal crystallization behavior, and mechanical properties of PVDF/xGNP nanocomposites was investigated.

EXPERIMENTAL

Materials and sample preparation

PVDF (Solef 6008) used in this study was purchased from Solvay (Shanghai). Natural flake graphite was provided by Qingdao Dingding graphite products factory. H_2SO_4, HNO_3, ethanol, and *N*,*N*-dimethylformamide (DMF) were purchased from Guangzhou Chemical Reagent Company and used directly without any further treatment.

The procedure for preparation of PVDF/xGnP nanocomposites is illustrated in Figure 1. Briefly, natural flake graphite was added into a mixed solution composed of sulfuric acid and nitric acid with a volume ratio of 4 : 1. After being stirred at room temperature for 24 h, the mixture was filtered, and the black solid was washed with deionized water until the pH value of the solution was up to 7. Subsequently, the acid-intercalated graphite was dried at 80°C for 24 h. The above dried graphite was expanded at 1000°C for 1 min in a muffle furnace to form expanded graphite. To obtain xGnPs, expanded graphite in 70% ethanol solution was subjected to

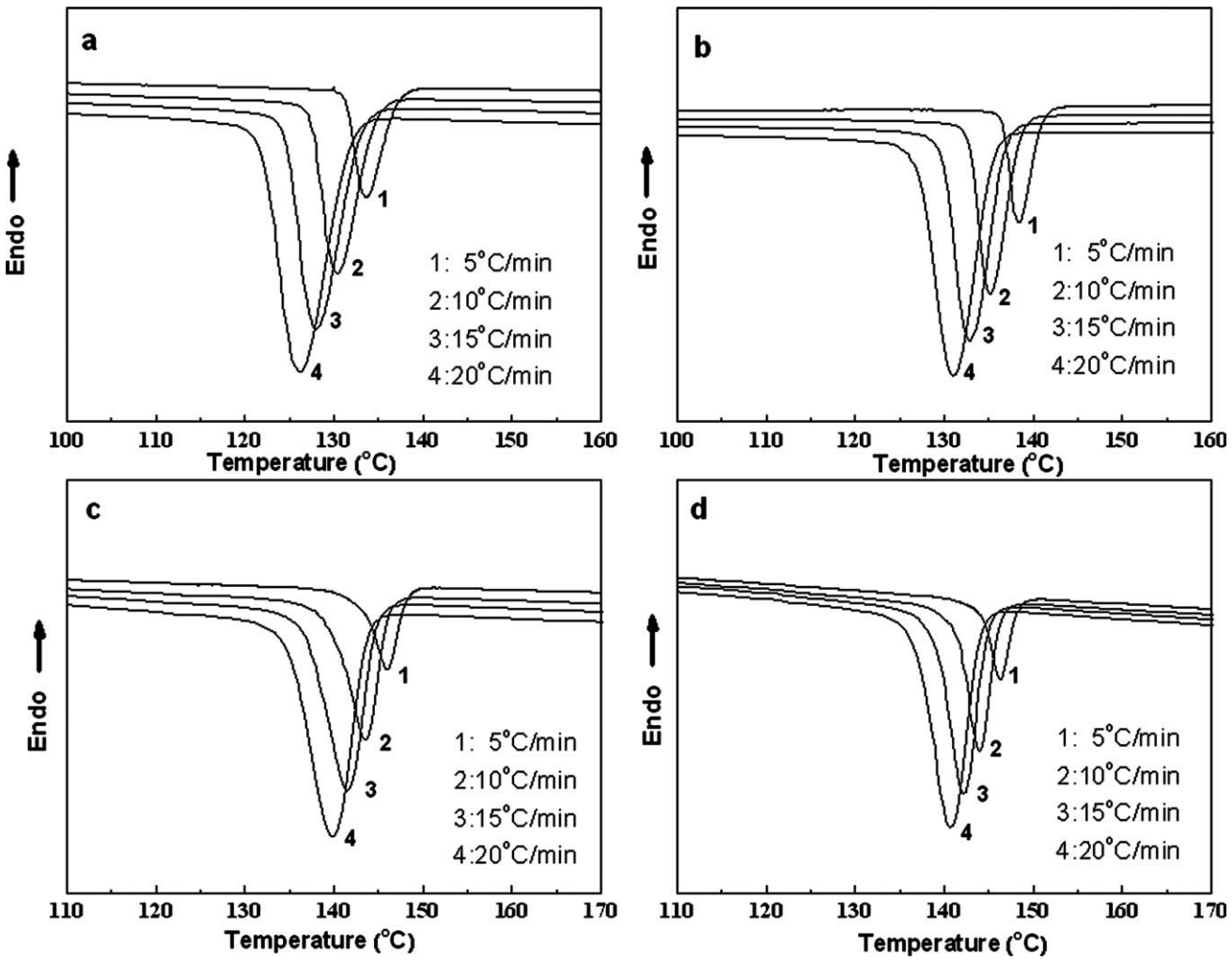

Figure 2 DSC curves of (a) PVDF, (b) PEG1, (c) PEG5, and (d) PEG10 at various cooling rates.

ultrasonic powdering for 6 h. The PVDF/xGnP nanocomposites were prepared by mixing desired amount of xGnP and PVDF in 100 mL of DMF solution at 80°C under stirring for 2 h and then treated with ultrasonic powdering for another 2 h. The mixture was poured into 200 mL of deionized water for rapid precipitation, and the product was kept in a vacuum oven at 70°C for 3 days. The samples with xGnP concentration of 1, 5, and 10 wt % were designated as PEG1, PEG5, and PEG10, respectively.

Characterization

Scanning electron microscopy (SEM, JEOL Model, JSM-6490) and transmission electron microscopy (TEM, JEOL Model, JEM-2010) were used to observe the microscopic structure of xGnP and PVDF/xGnP nanocomposites. Differential scanning calorimetry (DSC) thermal analysis was carried out with a Perkin Elmer DSC-7 differential scanning calorimeter under a nitrogen atmosphere. Sample was initially heated to 200°C at a rate of 10°C/min. It was held for 5 min at this temperature to eliminate previous thermal histories before cooling to 30°C at a specified cooling rate. After keeping at 30°C for 3 min, sample was reheated to 200°C at a heating rate of 10°C /min, followed by the next cooling and heating cycle. The cooling rates used were 5, 10, 15, and 20°C/min, respectively. Wide-angle X-ray diffraction (WAXD) analyses were performed using a high-solution X-ray diffractometer system (Bruker D8 Discover). Dynamic mechanical property was measured by a Perkin Elmer diamond dynamic mechanical analyzer lab system at a frequency of 1 Hz in a nitrogen atmosphere, with a temperature range from −80 to 80°C at a scan rate of 5°C/min.

RESULTS AND DISCUSSION

Distribution of xGnP in PVDF matrix

xGnPs were prepared by subjecting natural graphite flake to acidic intercalation, rapid thermal treatment, and ultrasonic powdering in sequence, which has

TABLE I
Values of T_p, ΔH_c, and α for PVDF and Its Nanocomposites

Sample	Cooling rate (°C/min)	T_p (°C)	ΔH_c (J/g)	α (%)
PVDF	5	133.68	46.39	44.35
	10	130.28	45.73	43.72
	15	127.97	46.18	44.14
	20	125.99	47.22	45.14
PEG1	5	138.84	43.81	41.88
	10	135.11	44.45	42.49
	15	132.97	44.71	42.74
	20	130.99	45.64	43.63
PEG5	5	145.99	40.11	38.34
	10	143.43	41.71	39.87
	15	141.45	43.06	41.17
	20	139.97	43.25	41.35
PEG10	5	146.31	37.84	36.18
	10	143.9	40.25	38.48
	15	142.16	41.78	39.94
	20	140.59	42.11	40.26

been described in detail in the experimental part. As shown in Figure 1, the obtained graphite nanoplates have a size of 20–60 nm in thickness and 0.5–25 μm in diameter. To investigate the dispersion state of xGnP in the PVDF matrix, sample PEG1 was observed by TEM. The result shows that most of the graphite nanoplates are isolated and evenly distributed within the PVDF matrix. Moreover, from the SEM images of the fractured PVDF/xGnP nanocomposites for sample PEG1, it can be seen that xGnPs were embedded in the PVDF matrix. According to the FTIR results reported by other groups,[7,10] there are some functional groups, such as C—O—C, C—OH, and COOH, on the surface of xGnP. The existence of these functional groups can have interaction with the PVDF molecular chains possessing the strong polar group F, leading to the well dispersion of xGnP in the PVDF matrix.

Nonisothermal crystallization analysis

Figure 2 shows crystallization curves for pure PVDF and its nanocomposites at different cooling rates. The peak crystallization temperature (T_p), the heat of crystallization (ΔH_c), and the crystallinity degree (α) of pure PVDF and its nanocomposites can be obtained from these curves, and the results are listed in Table I. The degree of crystallinity (α) can be calculated by

$$\alpha(\%) = \frac{\Delta H_c}{(1-\Phi)\Delta H_c^0} \times 100, \quad (1)$$

where ΔH_c^0 is the heat of fusion for 100% crystalline PVDF and Φ is the weight fraction of xGnP in the nanocomposites. A value of 104.6 J/g was used for ΔH_c^0 as the heat of fusion of 100% crystalline PVDF.[18] From Table I, it is clear that the T_p values of all nanocomposites are higher than those of pure PVDF and increase with increasing xGnP content at a given cooling rate. For example, at the cooling rate of 20°C/min, T_p values for PEG1, PEG5, and PEG10 are 130.99, 139.97, 140.59°C, respectively, whereas for pure PVDF, it is only 125.99°C. This phenomenon can be explained by the heterogeneous nucleation effect of the xGnPs on PVDF macromolecule segments, which leads to the crystallization of PVDF at a higher temperature. On the other hand, the X_c values of nanocomposites at various cooling rates were lower than those of pure PVDF, implying that the degree of crystallization for PVDF/xGnP nanocomposites was reduced. This phenomenon may be attributed to the interface interaction between PVDF and xGnP, which would reduce the motion ability of PVDF chains.[19]

Activation energy and nucleation activity for nonisothermal crystallization

Kissinger[20] has suggested a method to determine the activation energy for the transport of the macromolecular segments to the growing surface based on the plot of the following form:

$$\frac{d[\ln(\beta/T_p^2)]}{d(1/T_p)} = -\frac{\Delta E}{R}, \quad (2)$$

where R is the gas constant and β is the cooling rate. Figure 3 illustrates the plots of $\ln(\beta/T_p^2)$ vs. $1/T_p$ for PVDF and its nanocomposites. The activation energy can be calculated from the slopes of the plots, and the results are listed in Table II. The values of ΔE for PVDF/xGnP nanocomposites are all

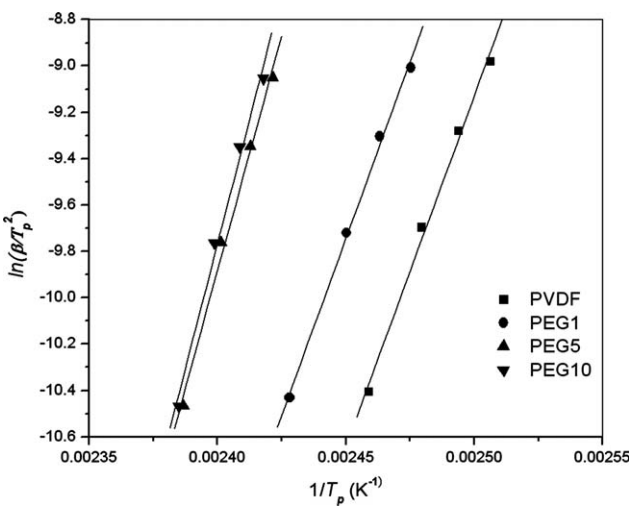

Figure 3 Plots of $\ln(\beta/T_p^o)$ against $1/T_P$ for PVDF and its nanocomposites.

TABLE II
Values of ΔE and ε for PVDF and Its Nanocomposites

Sample	ΔE	ε
PVDF	251.55	–
PEG1	254.06	0.67
PEG5	337.61	0.34
PEG10	358.55	0.33

higher than that of pure PVDF and increase with the increasing of xGnP content, implying that PVDF chain segments require more energy to move during the nonisothermal crystallization process because of the presence of xGnP. It suggests that the functional groups of xGnP may have some interaction with PVDF chain segments and then impede their movement to the growing crystalline surface, thus resulting in crystallization difficulty.[21]

The nucleating activity of xGnP in the PVDF/xGnP nanocomposites was determined by using the method suggested by Dobreva and Gutzow.[22,23] According to them, for homogeneous nucleation from the melt, the cooling rate can be written as follows:

$$\log \beta = \text{const} - \frac{B^0}{2.3\Delta T_p^2}, \tag{3}$$

whereas for the heterogeneous case,

$$\log \beta = \text{const} - \frac{B*}{2.3\Delta T_p^2}, \tag{4}$$

where ΔT_p is equal to $T_m - T_p$ (T_m: melting temperature), and B (B^0 and B^*) is a parameter related to three-dimensional nucleation, which can be calculated from the following equation:

$$B = \frac{\omega\sigma^3 V_m^2}{3nkT_m\Delta S_m^2}, \tag{5}$$

where n is the Kolmogorov–Avrami exponent, V_m is the molar volume of the crystallizing polymer, ΔS_m is the entropy of melting, k is the Boltzmann constant, σ is the specific surface energy, and ω is a geometrical factor.

The nucleation activity (ε) of the filler is defined as the ratio of B^* to B^0 ($\varepsilon = B^*/B^0$) and can be determined from the slopes of linear plots of log β vs. $1/\Delta T_p^2$. The value of ε approaches 0 if the filler is extremely active for nucleation, whereas approaches 1 for an absolutely inert filler. The plots of log β vs. $1/\Delta T_p^2$ for PVDF and its nanocomposites are shown in Figure 4, and the values of ε are given in Table II. The nucleation activity values were calculated as 0.67, 0.34, and 0.33 for PEG1, PEG5, and PEG10, respectively. This result shows that xGnP is an effective nucleation agent in the PVDF matrix, and the nucleation ability increases with increasing xGnP loading amount. According to the results of activation energy and nucleation activity, xGnPs may play two roles in the crystallization process of PVDF: heterogeneous nucleating agents to facilitate crystallization and obstacles to hinder the motion of PVDF molecular chains during crystallization process.[24]

Nonisothermal crystallization kinetics

To further understand the evolution of nonisothermal crystallization process, the Ozawa and modified Avrami–Ozawa methods were used to analyze the nonisothermal crystallization kinetics of PVDF and its nanocomposites.[25–27] Both Ozawa and modified Avrami–Ozawa methods are based on the Avrami equation used to describe the isothermal crystallization[28]:

$$X_t = 1 - \exp(-(Z_t t)^n). \tag{6}$$

The double natural logarithm of the Avrami equation gives the following relationship:

$$\ln[-\ln(1 - X_t)] = \ln Z_t + n \ln t, \tag{7}$$

where t is the crystallization time, X_t is the relative degree of crystallinity at time t, the exponent n is a mechanism constant with a value depending on the type of nucleation and the growth process, and the parameter Z_t is a growth rate constant involving both nucleation and growth rate parameters. From the DSC curves of melting crystallization (see Fig. 2),

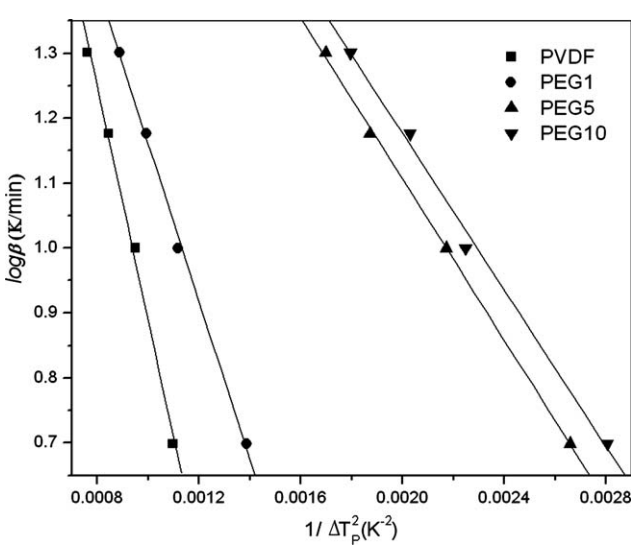

Figure 4 Plots of log β against $1/T_P^2$ for PVDF and its nanocomposites.

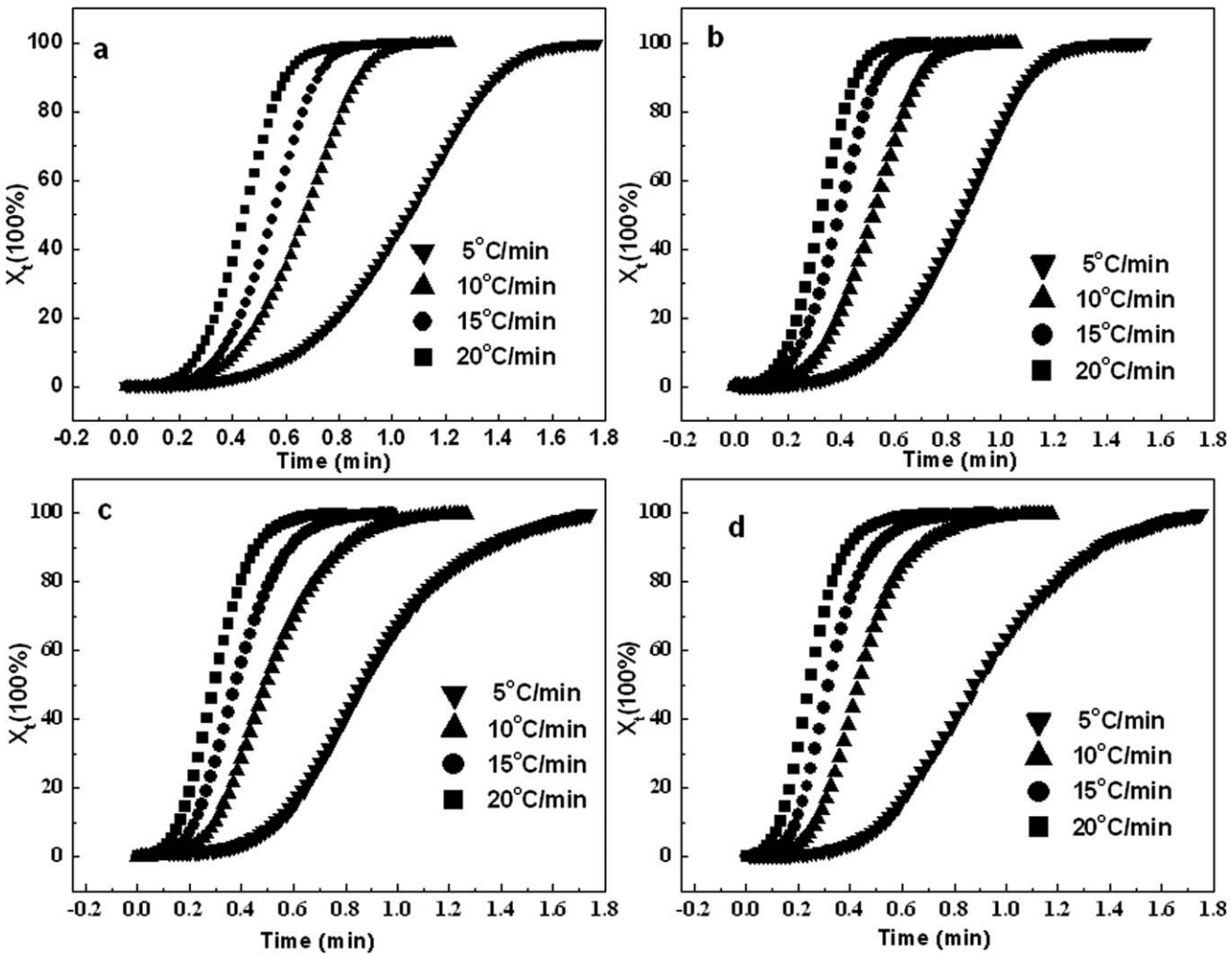

Figure 5 The variation of relative crystallinity degree as a function of time for (a) PVDF, (b) PEG1, (c) PEG5, and (d) PEG10 at various cooling rates.

the values of X_t at different time can be calculated according to the following equations:

$$X_T = \frac{\int_{T_0}^{T} (dH_c/dT)dT}{\int_{T_0}^{T_\infty} (dH_c/dT)dT}, \quad (8)$$

$$t = (T_0 - T)/\beta, \quad (9)$$

where X_T is the relative degree of crystallinity at temperature T, dH_c/dT is the heat flow rate, T_0 and T_∞ represent the onset and end of crystallization temperatures, respectively. By combining eq. (8) with eq. (9), the development of relative crystallinity X_t of PVDF and its nanocomposites with time t at different cooling rates can be obtained, as shown in Figure 5.

Assuming that the polymer melt was cooled at a constant rate and the mathematical derivation of Evans was valid, Ozawa[29] extended the Avrami equation to the nonisothermal condition:

$$X_T = 1 - \exp(-K(T)/\beta^m), \quad (10)$$

where K is the Ozawa crystallization rate constant and m is the Ozawa exponent. The double natural logarithm of the Ozawa equation gives the following relationship:

$$\ln[-\ln(1 - X_T)] = \ln K(T) - m \ln \beta. \quad (11)$$

A plot of $\ln[-\ln(1-X_T)]$ vs. $\ln \beta$ at a given temperature should yield a straight line if the Ozawa method is valid. Thus, $K(T)$ and m can be obtained from the intercept and the slope of the lines, respectively. The Ozawa plots of $\ln[-\ln(1-X_T)]$ vs. $\ln \beta$ for PVDF and its nanocomposites are shown in Figure 6. However, the obvious curvatures in the plots indicate that the Ozawa method cannot fit the crystallization behavior of PVDF and its nanocomposites, which can be ascribed to the factors such as the secondary crystallization of PVDF, the dependence of

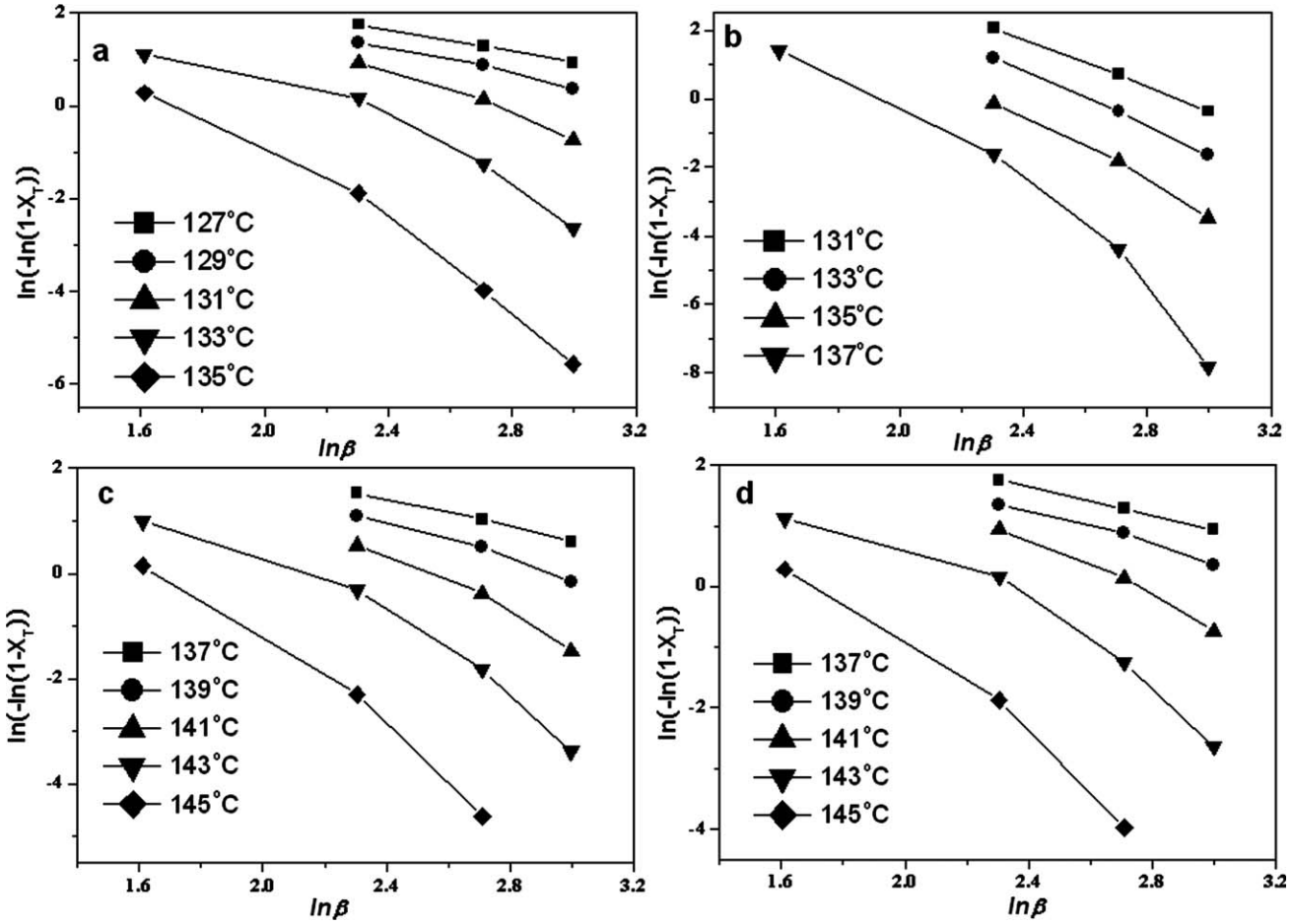

Figure 6 Ozawa plots of ln[−ln(1−XT)] against lnβ for crystallization of (a) PVDF, (b) PEG1, (c) PEG5, and (d) PEG10.

lamellar thickness on crystallization temperature, and the constant value of cooling function over the entire crystallization process.[30]

Mo and coworkers[31] proposed that the relation between β and t could be defined under a certain crystallinity degree because X_t (or X_T) was related to β and the crystallization time t (or temperature T). Using eq. (9) and combining eqs. (7) and (11), the following equation can be obtained for a given degree of crystallinity:

$$\ln k + n \ln t = \ln K(T) - m \ln \beta \tag{12}$$

and by rearrangement

$$\ln \beta = \ln F(T) - \alpha \ln t, \tag{13}$$

where $F(T) = [K(T)/k]^{1/m}$, which refers to the cooling rate that must be selected within a unit of crystallization time when the nonisothermal crystallization process reaches a certain degree of crystallinity, and α is the ratio of the Avrami exponent (n) to the Ozawa exponent (m), that is, n/m. It can be seen that $F(T)$ has a definite physical and practical meaning. According to eq. (13), at a given degree of crystallinity, plotting ln β vs. ln$t$ should result in a linear relationship. The kinetic parameter $F(T)$ and α can be determined from the intercept and the slope of the lines, respectively. As presented in Figure 7, modified Avrami–Ozawa plots of ln β vs. ln$t$ at different degree of crystallinity for PVDF and its nanocomposite show a good linearity, which confirms the advantage of this method applied in the PVDF/xGnP nanocomposites. The values of ln $F(T)$ and α are listed in Table III. It can be seen that the values of ln $F(T)$ for PVDF/xGnP nanocomposites are smaller than that for pure PVDF at the same degree of crystallinity, indicating that the addition of graphite nanoplates can accelerate the overall crystallization process of PVDF. Moreover, the ln $F(T)$ values of PVDF/xGnP nanocomposites appear to decrease with an increment in the graphite nanoplate content. In general, the crystallization process of polymer involves two steps: (a) the diffusion of crystallizable molecular chains to the crystal front and (b) nucleation. As discussed above, the xGnP can not only act as a heterogeneous nucleating agent to facilitate the formation of PVDF crystalline but also retard the

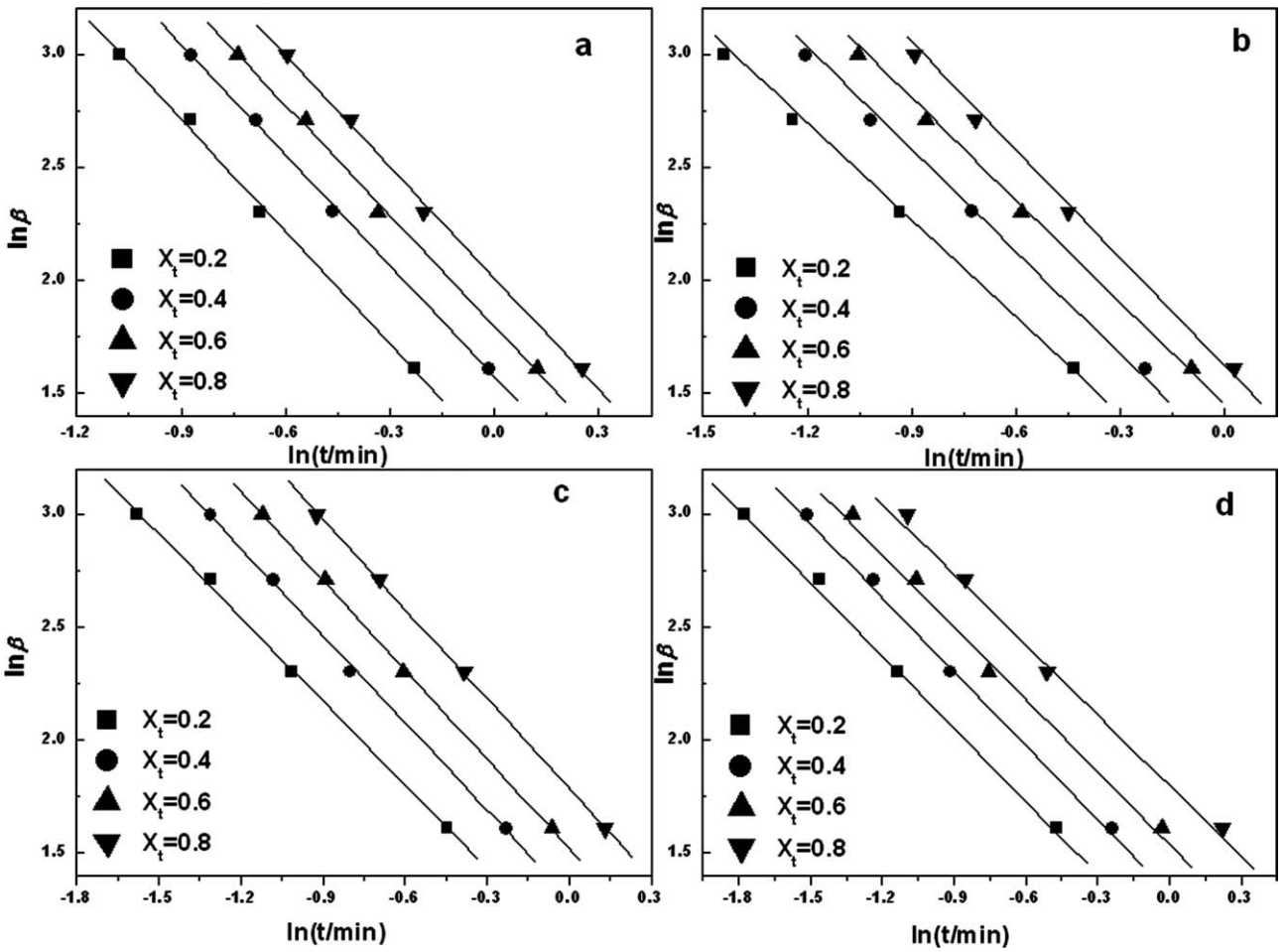

Figure 7 Modified Avrami–Ozawa plots of lnβ against for crystallization of (a) PVDF, (b) PEG1, (c) PEG5, and (d) PEG10.

movement of molecular chains due to the interaction between PVDF and xGnP. Therefore, under the conjunct influences of these two factors, sample PEG1 has the greatest crystallization ability with a minimum ln *F(T)* value among the PVDF/xGnP nanocomposites.

Melting following nonisothermal crystallization

To investigate the crystalline structures formed during the nonisothermal crystallization process, the subsequent heating of the samples cooled at different rates was performed at a rate of 10°C/min. As shown in Figure 8, pure PVDF evidently exhibits a shoulder melting peak at higher temperature. The existence of double melting peaks during DSC heating has generally been explained in two ways: recrystallization and polymorphism. According to the WAXD result (see Fig. 9), after being cooled from 200 to 30°C at a rate of 20°C/min, the crystallization structure of pure PVDF was dominated by α-form crystal as shown from the characteristic peaks at 2θ values of 17.6°, 18.3°, 19.9°, and 26.6° corresponding to α (020), α (100), α (110), and α (021), respectively. Therefore, the double melting peaks of pure PVDF did not originate from polymorphism, but from the melting of the recrystallized crystallites

TABLE III
Nonisothermal Crystallization Kinetics Parameters Obtained from the Modified Avrami–Ozawa Equation for PVDF and Its Nanocomposites

Sample	X_t	α	ln *F(T)*
PVDF	0.2	1.65	1.23
	0.4	1.63	1.58
	0.6	1.62	1.79
	0.8	1.64	2.01
PEG1	0.2	1.37	1.01
	0.4	1.41	1.27
	0.6	1.44	1.46
	0.8	1.50	1.63
PEG5	0.2	1.23	1.06
	0.4	1.28	1.30
	0.6	1.31	1.52
	0.8	1.31	1.78
PEG10	0.2	1.07	1.10
	0.4	1.09	1.33
	0.6	1.08	1.55
	0.8	1.05	1.81

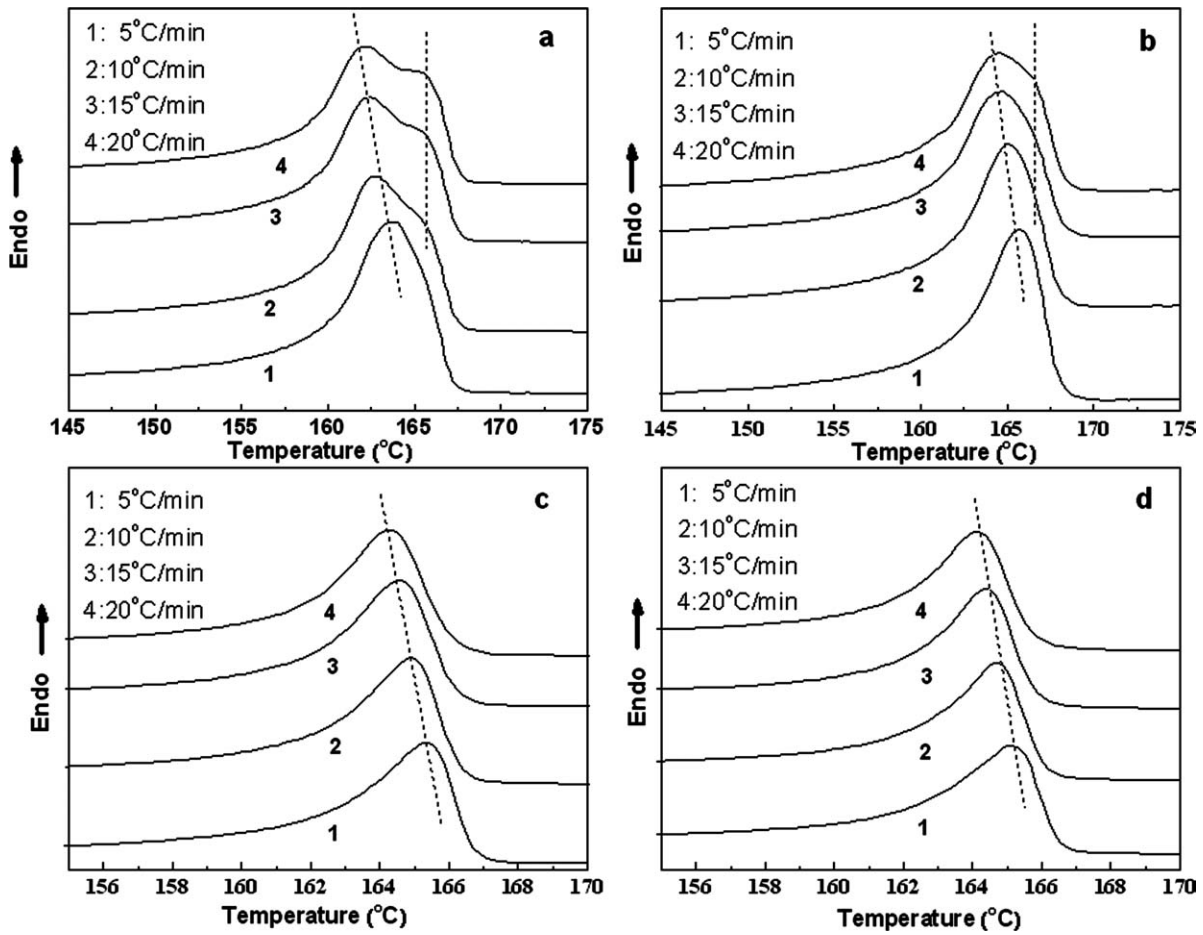

Figure 8 DSC melting curves of (a) PVDF, (b) PEG1, (c) PEG5, and (d) PEG10 following nonisothermal crystallization at different cooling rates.

formed during the subsequent heating scan. However, for sample PEG1, the intensity of shoulder melt peak became weaker, whereas sample PEG5 and PEG10 only show a single melting peak. The melting behavior of the PVDF/xGnP nanocomposites means that the good dispersion of graphite nanoplates in PVDF matrix induces homogeneous crystallization structure formation. [31–33]

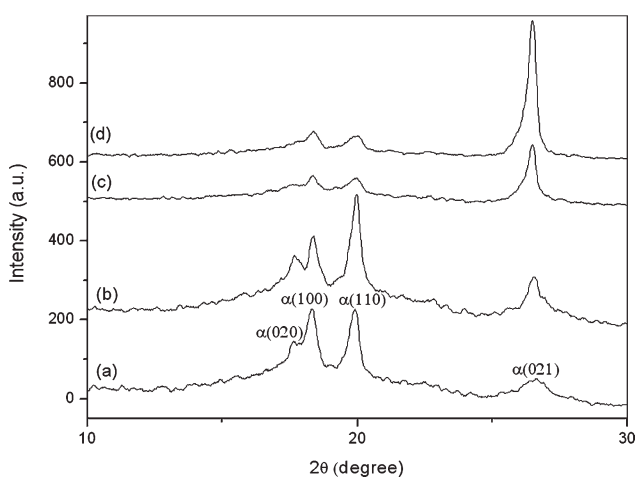

Figure 9 The WAXD results of (a) PVDF, (b) PEG1, (c) PEG5, and (d) PEG10 after being cooled from 200 to 30°C at a rate of 20°C/min.

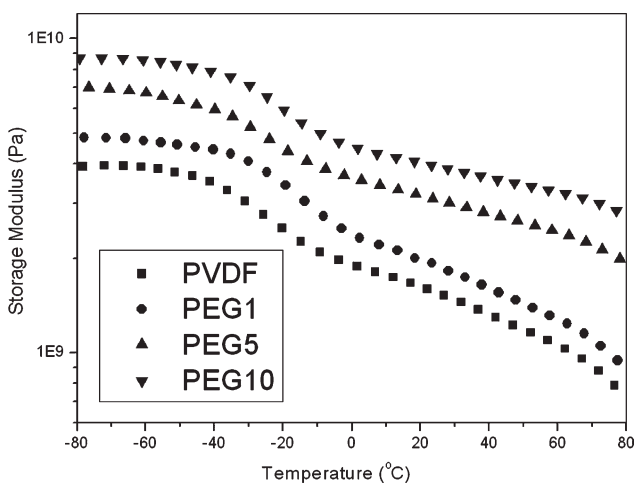

Figure 10 The variation of storage modulus as a function of temperature for PVDF and its nanocomposites with different xGnP loading.

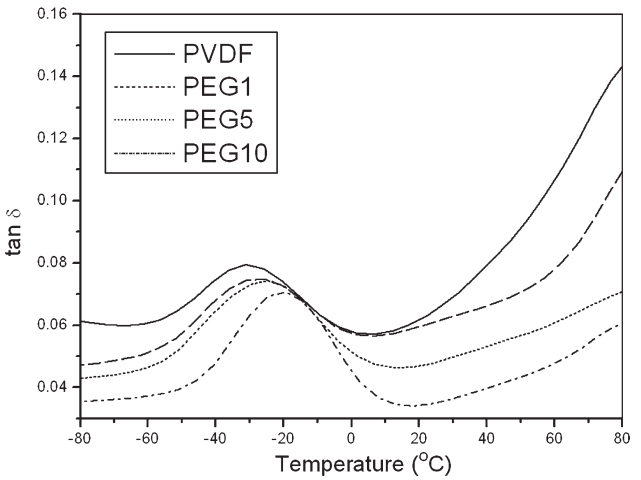

Figure 11 The variation of loss tangent as a function of temperature for PVDF and its nanocomposites with different xGnP loading.

Dynamic mechanical behavior

Figure 10 shows the storage moduli of PVDF and its nanocomposites. Although the storage moduli of all samples decreased with the increment of temperature over the temperature range between −80 and 80°C, the storage modulus of PVDF is significantly enhanced by the addition of xGnP at each temperature investigated, and sample PEG10 exhibits the largest storage modulus. This confirms that the presence of xGnP improves the dynamic mechanical property of PVDF. Figure 11 shows the tan Δ curves for PVDF and its nanocomposites. The tan Δ peak for pure PVDF at about −30°C corresponds to the glass transition temperature. For the PVDF/xGnP nanocomposites, the tan Δ peak shifted to a higher temperature and the peak intensity decreased with increasing xGnP content. The shift of the tan Δ peak to a higher temperature may be ascribed to the interaction between the xGnP and PVDF matrix, which hindered the motion of the polymer chains. A similar result has been reported for polyamide/clay nanocomposites by Tjong and Bao.[24]

CONCLUSIONS

Nanocomposites composed of PVDF and xGnP were prepared by solution precipitation method. The nanoscale dispersion of xGnP in PVDF matrix was confirmed by SEM and TEM. DSC has been used to investigate the influence of graphite nanoplates on the nonisothermal crystallization behavior of PVDF/xGnP nanocomposites. Two methods, including Ozawa and modified Avrami–Ozawa models, were used to analyze the nonisothermal crystallization kinetic of the nanocomposites. It was found that Ozawa method failed to provide an adequate description for the nonisothermal crystallization of PVDF and its nanocomposites, but the modified Avrami–Ozawa model has been proven to be successful. The graphite nanoplates in nanometer size might act as the nucleating agents and accelerated the overall nonisothermal crystallization process of PVDF especially when the xGnP loading amount was 1 wt %. Dynamic mechanical analysis indicated significant improvements in storage modulus over a temperature range of −80 to 80°C for PVDF/xGnP nanocomposites in comparison with pure PVDF.

References

1. Kuo, S. W.; Huang, W. J.; Huang, S. B.; Kao, H. C.; Chang, F. C. Polymer 2003, 44, 7709.
2. Jin, Y. H.; Park, H. J.; Im, S. S.; Kwak, S. Y.; Kwak, S. Macromol Rapid Commun 2002, 23, 135.
3. Zanetti, M.; Bracco, P.; Costa, L. Polym Degrad Stab 2004, 85, 657.
4. Gopakumar, T. G.; Lee, J. A.; Kontopoulou, M.; Parent, J. S. Polymer 2002, 43, 5483.
5. Alexandre, M.; Dubois, P.; Sun, T.; Garces, J. M.; Jerome, R. Polymer 2002, 43, 2123.
6. Zhao, C. G.; Feng, M.; Gong, F. L.; Qin, H. L.; Yang, M. S. J Appl Polym Sci 2004, 93, 676.
7. Chen, G. H.; Weng, W. G.; Wu, D. J.; Wu, C. L.; Lu, J. R.; Wang, P. P.; Chen, X. F. Carbon 2004, 42, 753.
8. Chen, G. H.; Weng, W. G.; Wu, D. J.; Wu, C. L. Eur Polym J 2003, 39, 2329.
9. Miloaga, D. G.; Hosein, H. A. A.; Misra, M.; Drzal, L. T. J Appl Polym Sci 2007, 106, 2548.
10. Zheng, G. H.; Wu, J. S.; Wang, W. P.; Pan, C. Y. Carbon 2004, 42, 2839.
11. Weng, W. G.; Chen, G. H.; Wu, D. J. Polymer 2003, 44, 8119.
12. Kalaitzidou, K.; Fukushima, H.; Drzal, L. T. Carbon 2007, 45, 1446.
13. Yang, H.; Tian, M.; Jia, Q. X.; Shi, J. H.; Zhang, L. Q.; Lim, S. H.; Yu, Z. Z.; Mai, Y. W. Acta Mater 2007, 55, 6372.
14. Li, L. W.; Luo, Y. L.; Li, Z. Q. Smart Mater Struct 2007, 16, 1570.
15. Yee, W. A.; Kotaki, M.; Liu, M. Y.; Lu, X. H. Polymer 2007, 48, 512.
16. Wang, M.; Shi, J. H.; Pramoda, K. P.; Goh, S. H. Nanotechnology 2007, 18, 235701.
17. He, F. A.; Lau, S. T.; Chan, H. L. W.; Fan, J. T. Adv Mater 2009, 21, 710.
18. Nakagawa, K.; Ishid, A. Y. J Polym Sci Polym Phys Ed 1973, 11, 2153.
19. He, F. A.; Zhang, L. M.; Yang, F.; Chen, L. S.; Wu, Q. J Polym Res 2006, 13, 483.
20. Kissinger, H. E. J Res Natl Bur Stand 1956, 157, 217.
21. Liu, Q.; Peng, Z. Q.; Chen, D. J. Polym Eng Sci 1956, 47, 460.
22. Dobreva, A.; Gutzow, I. J Non-Cryst Solids 1993, 162, 1.
23. Dobreva, A.; Gutzow, I. J Non-Cryst Solids 1993, 162, 13.
24. Tjong, S. C.; Bao, S. P. J Polym Sci Part B: Polym Phys 2004, 42, 2878.
25. Xia, X. P.; Xie, C. S.; Cai, S. Z. Thermochim Acta 2005, 427, 29.
26. Xu, W.; Ge, M.; He, P. J Appl Polym Sci 2001, 82, 2281.
27. He, F. A.; Fan, J. T.; Lau, S. T. Polym Test 2008, 27, 964.
28. Avrami, M. J Chem Phys 1939, 7, 1103.
29. Ozawa, T. Polymer 1971, 12, 50.
30. Joshi, M.; Butola, B. S. Polymer 2004, 45, 4953.
31. Liu, T. X.; Mo, Z. S.; Wang, S. G.; Zhang, H. F. Polym Eng Sci 1997, 37, 568.
32. Gao, Y.; Wang, Y.; Shi, J.; Bai, H. W.; Song, B. Polym Test 2008, 27, 179.
33. Apiwanthanakorn, N.; Supaphol, P.; Nithitanakul, M. Polym Test 2004, 23, 817.